Photophysical and photochemical processes followed by 320 nm femtosecond laser excitation of IrCl$_6^{2-}$ complex in aqueous and methanol solutions

Evgeni M. Glebov [a,b,*], Ivan P. Pozdnyakov [a,b], Alexey A. Melnikov [c], Sergey V. Chekalin [c]

[a] *Voevodsky Institute of Chemical Kinetics and Combustion, Siberian Branch of the Russian Academy of Sciences, Novosibirsk 630090, Russian Federation*
[b] *Novosibirsk State University, Novosibirsk 630090, Russian Federation*
[c] *Institute of Spectroscopy, Russian Academy of Sciences, Troitsk, 142190 Moscow, Russian Federation*

ABSTRACT

Ultrafast pump-probe spectroscopy (λ_{pump} = 320 nm) was applied to study the primary photochemical processes for IrCl$_6^{2-}$ complex in aqueous and methanol solutions. The excitation to the mixed LMCT and d–d states was followed by formation of an intermediate absorption completely decaying with the characteristic time of 20–30 ps. The almost complete recovery of the ground state is consistent with the low photochemical activity caused by the excitation of IrCl$_6^{2-}$ into the region of the near UV bands. Comparison with the recently published results on the visible excitation of the complex is presented.

© 2014 Elsevier B.V. All rights reserved.

1. Introduction

Photochemistry of hexahalide complexes of tetravalent platinum metals is two hundred years old [1]. In the XX century these complexes were considered as objects of photochemistry interesting from the academic point of view solely [2–5]. Currently photochemistry of haloid complexes of platinum metals has received a new stimulus for development caused by two practical tasks. The first task comes from the field of photocatalysis. A fundamental problem there is to expand absorption spectra of semiconductors (TiO$_2$, CdS) into the visible spectral region. One of the possibilities to solve this problem is the modification of TiO$_2$ [6–9] and CdS surface [10,11] by platinum metal complexes. For complete description of processes in these systems, photochemistry of complexes formed by desorbed metal in the solution bulk should also be taken into account [7].

Another aspect of interest to the photochemistry of platinum metals complexes is caused by photodynamic therapy (PDT), which is a prospective way to combine the cytotoxicity of platinum metals and the advantages of photodynamic therapy (selectivity and low toxicity) [14]. Typically the complexes of platinum are used in PDT [12–14]. Anti-tumor activity of iridium [15–17] and the use of its complexes for PDT [18,19] were also reported.

Typically, the reaction mechanisms in photochemistry of coordination compounds were proposed based on the results of stationary experiments [2–5]. Often, the participation of the short-living reactive intermediates, like Adamson's radical pairs [20], was postulated. Nowdays, these mechanisms could be examined by means of time-resolved methods starting from the femtosecond resolution, and the existence of proposed intermediates could be either supported or refuted. As a result, the whole reaction path, from ultrafast processes to final products, could be followed, and the complete reaction pathways could be established. Recently, some of the hexahalide complexes of platinum metals were the subjects of femtosecond studies. Ultrafast pump-probe spectroscopy was applied to determine the primary photophysical and photochemical processes for PtBr$_6^{2-}$ [21–25], PtCl$_6^{2-}$ [24,25], IrCl$_6^{2-}$ [26,27], IrBr$_6^{2-}$ [23,28] and OsBr$_6^{2-}$ [23] complexes. Photoaquation of PtBr$_6^{2-}$ gives an example of refinement of the reaction mechanism based on femtosecond experiments.

* Corresponding author at: Siberian Branch of the Russian Academy of Sciences, Voevodsky Institute of Chemical Kinetics and Combustion, 630090 Novosibirsk, Russian Federation. Tel.: +7 383 3332385; fax: +7 383 3307350.
E-mail addresses: glebov@kinetics.nsc.ru, glebov@ns.kinetics.nsc.ru (E.M. Glebov).

Table 1
Spectroscopy and photochemistry of hexahalide complexes of Ir(IV) in aqueous and methanol solutions.

Wavelength (nm)	Absorption bands	Transitions	Photochemical Properties	
			H_2O	CH_3OH
320	Maximum at 306 nm	LMCT $\pi(t_{1u}) \rightarrow d(t_{2g})$ [35,36] superimposed with d–d $d(t_{2g}) \rightarrow d(e_g^*)$ [34]	Photoaquation $\varphi_{aq} = 0.01$ [30]	Photoreduction $\varphi_{red} = 0.1$ [37]
400–420	Maxima at 415 nm and 432 nm	LMCT $\pi(t_{2u}) \rightarrow d(t_{2g})$ [34]	No reaction [30]	No reaction [37]

Traditionally it was thought that the photoaquation of this complex occurs through the lowest excited triplet state [29]. Recently Zheldakov et al. [22,23] reported that the mentioned triplet state is dissociative, and the participation of pentacoordinated Pt(IV) intermediates was established.

In our previous works on the ultrafast kinetic spectroscopy of $PtBr_6^{2-}$ [21,24,25], $PtCl_6^{2-}$ [24,25] and $IrCl_6^{2-}$ [26,27] complexes the excitation at the spectral region of 400–420 nm was used. The photochemical behavior of any of these complexes significantly depends on the excitation wavelength. For example, the quantum yield of $IrCl_6^{2-}$ photoaquation [30,31] is wavelength-dependent. In this work, the 320 nm excitation was applied to study the ultrafast processes for $IrCl_6^{2}$ in aqueous and methanol solutions. The goal was to compare the processes caused by the excitation of the complex into the different electronic states.

2. Experimental

Ultrafast pump-probe spectroscopy was used to study transient absorption of the samples in femto- and picosecond time domains. The samples were excited by ~100 fs pulses at ~320 nm (fourth harmonic of a signal wave of TOPAS parametric amplifier). The instruments used were described in details elsewhere [32]. The excitation energy at 320 nm was ca. 1 μJ/pulse, the excitation pulse repetition rate was 1 kHz, and 200 pulses were used to record a single time-resolved spectrum. The investigated solutions (total volume of 10 ml) were pumped through a 1 mm cell at room temperature to provide uniform irradiation and avoid possible degradation due to photochemical reactions. The experimental data were globally fitted by two- or three-exponential models. The fitting program performed corrections of the group velocity dispersion and calculated the response time of the instrument.

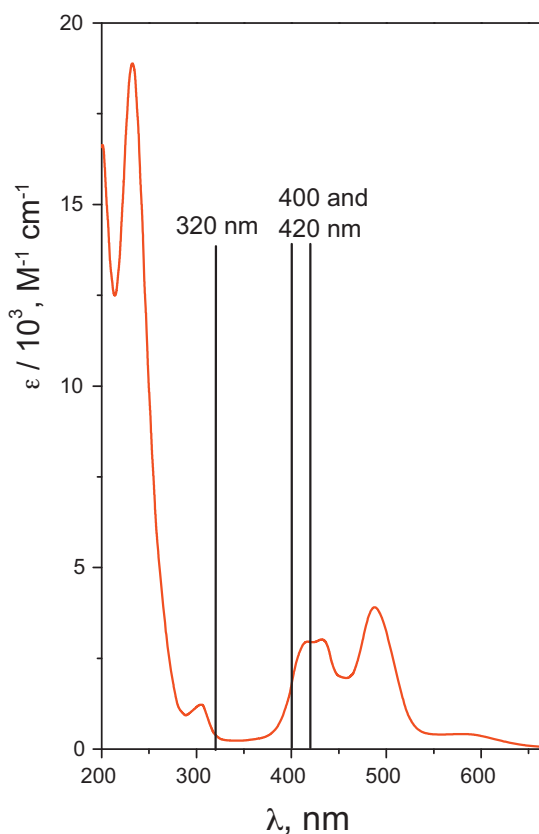Electronic absorption spectra were recorded using Agilent 8453 (Agilent Technologies) spectrophotometer.

Solutions of $IrCl_6^{2-}$ complex were prepared from the $Na_2IrCl_6 \times 6H_2O$ salt synthesized as described in [33]. Deionized water and methanol (Aldrich) were used for the sample preparation. Methanol was used without additional purification.

3. Results and discussions

3.1. UV spectra and photochemistry of $IrCl_6^{2-}$ complexes

The electronic absorption spectrum of $IrCl_6^{2-}$ in aqueous solution is shown in Fig. 1. In this figure, the wavelengths of femtosecond laser excitation used in this and previous papers are marked. The information on the nature of the targeted absorption bands is collected in Table 1. This table also provides the data on the photochemical processes caused by the excitation in the region of the bands of interest.
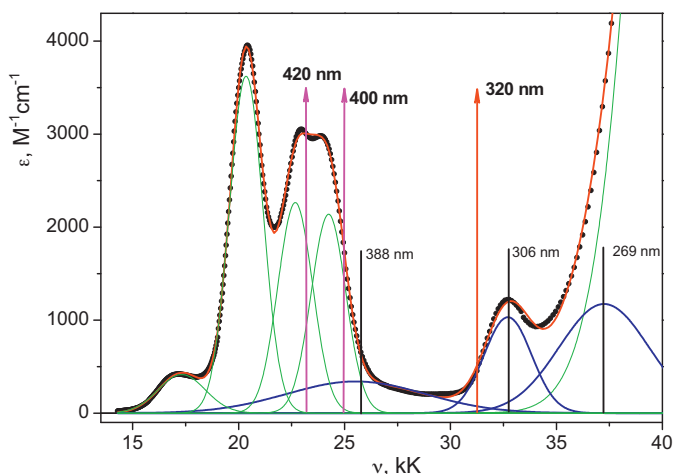
$IrCl_6^{2-}$ is a $5d^5$ low spin octahedral complex. Its UV spectrum (Fig. 1) contains strong absorption bands both in visible and UV regions. The simple assignment of the absorption bands

Fig. 1. Electronic absorption spectrum of the $IrCl_6^{2-}$ complex in aqueous solution. Excitation wavelengths used in ultrafast kinetic measurements are marked.

using non-relativistic symmetry was performed by Jørgensen [34]. According to [34], the absorption bands in the region of 400–500 nm with the extinction coefficient of ca. 4000 M^{-1} cm^{-1} are the bands of ligand-to-metal charge transfer (LMCT). Relatively weak ($\varepsilon \sim 1000 M^{-1} cm^{-1}$) band at 306 nm was assigned by Jørgensen to d–d ligand–field transitions [34], probably, superimposed with the LMCT transitions. Later, Goursot et al. [35] based on the relativistic theoretical calculations assigned this band as belonging to presumably LMCT transition, which was supported by Case and Lopez [36].

For comparison of the results of femtosecond experiments performed with different excitation it is necessary to analyze the absorption spectrum of $IrCl_6^{2-}$ more thoroughly. Fig. 2 shows the results of the spectrum deconvolution into eight Gaussian components (the deconvolution should be performed in wave numbers units). This procedure gives more or less satisfactorily fit of the experimental spectrum. Arrows in Fig. 2 correspond to excitation wavelengths used in different experiments, namely, 420 and 400 nm in works [26,27] and 320 nm in this work. We are most

Fig. 2. The UV absorption spectrum the $IrCl_6^{2-}$ complex in aqueous solution (black dots) and its deconvolution into eight Gaussian functions (red line). Blue lines—Gaussian components which could affect the 320 nm excitation (their centers are marked); green lines—other Gaussian components (the most energetic component is shown only partially). Excitation wavelengths used in ultrafast kinetic measurements in this work are marked by arrows. (For interpretation of the references to color in this figure legend, the reader is referred to the web version of this article.)

interested in 320 nm excitation. The Gaussian components which yield the absorption at this wavelength are marked in blue in Fig. 2.
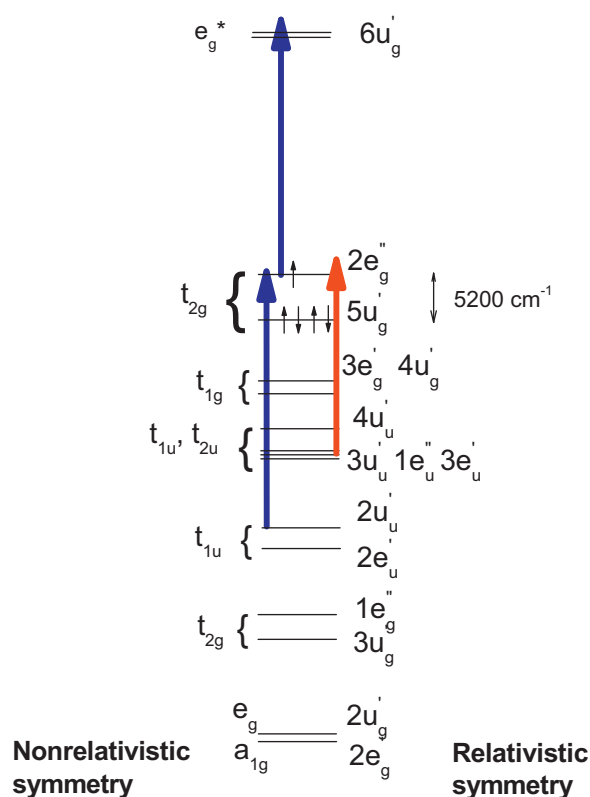
The approximate structure of molecular orbitals of the $IrCl_6^{2-}$ complex is shown in Fig. 3. Left-hand side numbering of the orbitals corresponds to the simple ligand field (LF) approximation for the octahedral $5d^5$ low spin complex [34]. Right-hand side numbering of the orbitals in Fig. 3 corresponds to the relativistic approximation [35,36]. The letters e and u mark the dimeric and tetrameric irreducible representations of the O_h symmetry group caused by spin–orbit coupling (this is an analogue of full momenta $j = 1/2$ and $j = 3/2$ for the case of spherical symmetry). Red arrow shows the 400 nm excitation, which corresponds to the low-energy LMCT band, and blue arrows show the 320 nm excitation which could correspond to both the LMCT and d–d and bands.

The 320 nm excitation of $IrCl_6^{2-}$ could result both in $2u_u' \rightarrow 2e_g''$ and $2e_g'' \rightarrow 6u_g'$ electron promotions (Fig. 3). In the case of $2u_u' \rightarrow 2e_g''$ promotion corresponding to the LMCT excitation, the formation of a hole in the $2u_u'$ orbital results in the formation of an only excited state $3U_u'$ [35,36]. This LMCT band is Laporte allowed and symmetry allowed; therefore, the absorption coefficient in the maximum of the 306 nm band ($1230\,M^{-1}\,cm^{-1}$, Fig. 2) is mainly provided by the charge transfer.

$2e_g'' \rightarrow 6u_g'$ promotion corresponding to the d–d excitation results in the formation of the excited configuration $t_{2g}^4 e_g^1$, which consists of two quartet and eight doublet terms [35]. Ten terms split into twenty terms allowed to spin-orbital interaction. According to the calculations of [35], these twenty ligand field states are spread along the spectrum from 250 to 500 nm being partly hidden under the more intense LMCT bands. In the deconvolution shown in Fig. 2, these states manifest itself in the two peaks with the maxima at 269 and 388 nm. Among 20 d–d excited states four terms are close to 320 nm excitation, namely $2E_g''$, $7U_g'$, $3E_g'$, and $8U_g'$ terms [35]. According to the ratio of Gaussian components at 306 and 388 nm (Fig. 2), the yield of the d–d bands to the total absorption at 320 nm is not more than 20%. Therefore, one can consider the excitation at this wavelength as presumably belonging to the near UV LMCT band.

Now let us briefly look through the photochemistry of the $IrCl_6^{2-}$ complex. The visible LMCT bands are not photoactive both in aqueous [27] and in alcohol [37] solutions. Excitation of aqueous
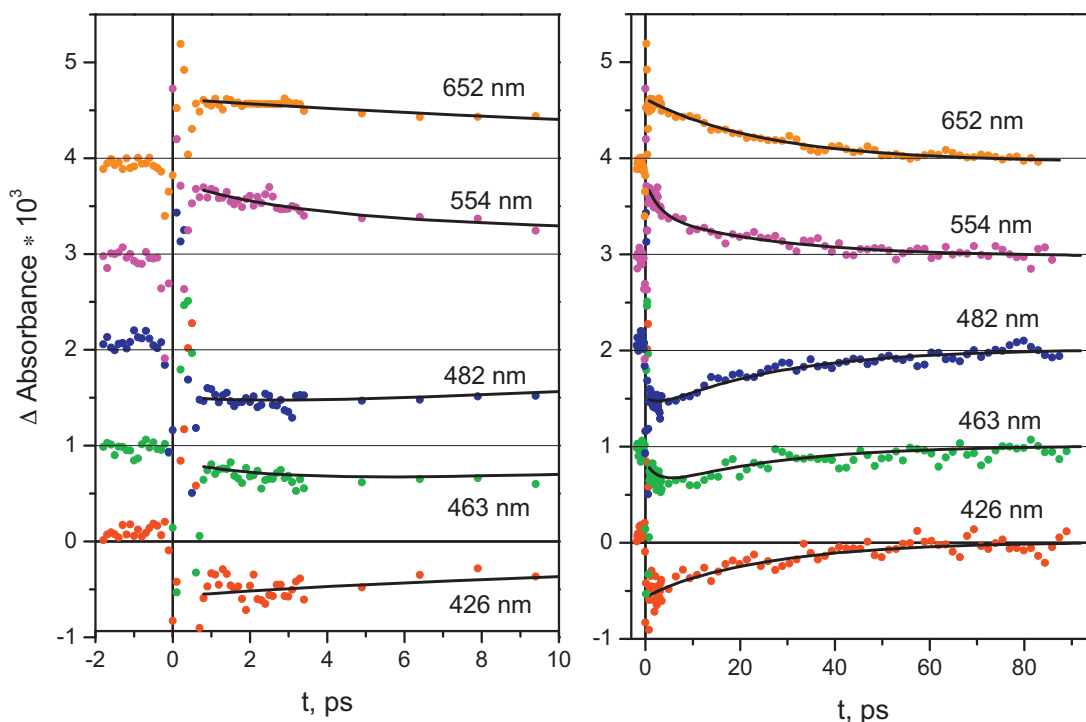

Fig. 3. The approximate structure of molecular orbitals of the $IrCl_6^{2-}$ complex according to [34] (non-relativistic approximation, left-hand side) and [35,36] (relativistic approximation, right-hand side). Electrons in filled orbitals lower than $5u_g'$ are not shown. Red arrow corresponds to 400 nm excitation. Blue arrows correspond to 320 nm excitation. (For interpretation of the references to color in this figure legend, the reader is referred to the web version of this article.)

solutions in the region of 313 nm results in photoaquation with the formation of $IrCl_5(H_2O)^-$ complex, but the quantum yield is rather low (ca. 0.01 [30]). Laser flash photolysis experiments with the nanosecond time resolution (308 nm) have shown that the formation of the final photoaquation products occurs less than for 50 ns [31]. The mechanism of photolysis caused by the near UV excitation seems to be the direct photoaquation (reactions (1) and (2), [30]), without any impact of redox processes. The low value of the quantum yield is determined by the ratio of the rate constants k_2/k_{-1}.

$$IrCl_6^{2-} \underset{k_{-1}}{\overset{h\nu}{\rightleftarrows}} (IrCl_6^{2-})* \tag{1}$$

$$(IrCl_6^{2-})* \xrightarrow[k_2]{H_2O} IrCl_5(H_2O)^- + Cl^- \tag{2}$$

Excitation in the vicinity of 313 nm in alcohol solutions results in photoreduction of Ir(IV) to Ir(III) with the formation of $IrCl_6^{3-}$ complex and hydroxyalkyl radicals [37,38]. The primary photochemical process in this case is an electron transfer from the solvent molecule to the light-excited complex (reaction (4)). The primary quantum yield of Ir(III) formation determined by reactions (3) and (4) is about 0.1 [38]. The reaction (5) between the hydroxyalkyl radical and the initial complex doubles the quantum yield of Ir(III) formation in oxygen-free solutions [37].

$$IrCl_6^{2-} \overset{h\nu}{\rightleftarrows} (IrCl_6^{2-})* \tag{3}$$

Fig. 4. (λ_{pump} = 320 nm) Photolysis of $IrCl_6^{2-}$ (1.9×10^{-3} M) in methanol solution. Experimental kinetic curves of transient absorption at different wavelengths and time domains. Solid lines are the best two-exponential fits (Eq. (6)) after reconvolution with the instrument response function.
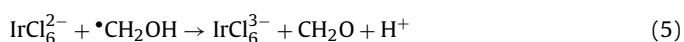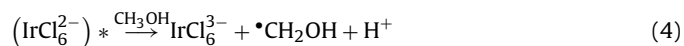
Table 2
Ultrafast kinetic spectroscopy of hexahalide complexes of Ir(IV) and Pt(IV) in water and methanol solutions[a].

Solvent	Excitation at 400–420 nm [26,27]						Excitation at 320 nm			
	τ_1 (fs)	Process	τ_2 (ps)	Process	τ_3 (ps)	Process	τ_1 (ps)	Process	τ_2 (ps)	Process
H_2O	500 ± 100	$2U_u'^* \rightarrow 1U_g'$	–		18 ± 2	$1U_g' \rightarrow 1E_g''$	0.6^b		20 ± 6	$1U_g' \rightarrow 1E_g''$
CH_3OH	350 ± 70	$2U_u'^* \rightarrow 1U_g'^*$	2.2 ± 0.5	$1U_g'^* \rightarrow 1U_g'$	30 ± 3	$1U_g' \rightarrow 1E_g''$	2.8 ± 2.0	$1U_g'^* \rightarrow 1U_g'$	26 ± 7	$1U_g' \rightarrow 1E_g''$

[a] Experimental errors were not provided in the original papers. They were introduced based on the analysis of the raw experimental data.

[b] Too few experimental points to extract this time.

$$\left(IrCl_6^{2-} \right)_* \xrightarrow{CH_3OH} IrCl_6^{3-} + {}^\bullet CH_2OH + H^+ \tag{4}$$

$$IrCl_6^{2-} + {}^\bullet CH_2OH \rightarrow IrCl_6^{3-} + CH_2O + H^+ \tag{5}$$

3.2. Kinetic curves and their fitting

The kinetic curves obtained in the experiments on the ultrafast pump-probe spectroscopy were globally fitted using either a biexponential function (6) or a triexponential function (7). The results are collected in Table 2. This table also carries the information concerning proposed interpretation of the observed processes.

$$\Delta A(\lambda, t) = A_1(\lambda)e^{-k_1 t} + A_2(\lambda)e^{-k_2 t} \tag{6}$$

$$\Delta A(\lambda, t) = A_1(\lambda)e^{-k_1 t} + A_2(\lambda)e^{-k_2 t} + A_3(\lambda)e^{-k_3 t} \tag{7}$$

When the kinetic curves are fitted using the triexponential function (7), the sequential decay of the transient absorption $A \rightarrow B \rightarrow C \rightarrow$ ground state was proposed. The species associated difference spectra (SADS) of the individual components were calculated by means of the formulae derived in [39].

$$S_A(\lambda) = A_1(\lambda) + A_2(\lambda) + A_3(\lambda) \tag{8}$$

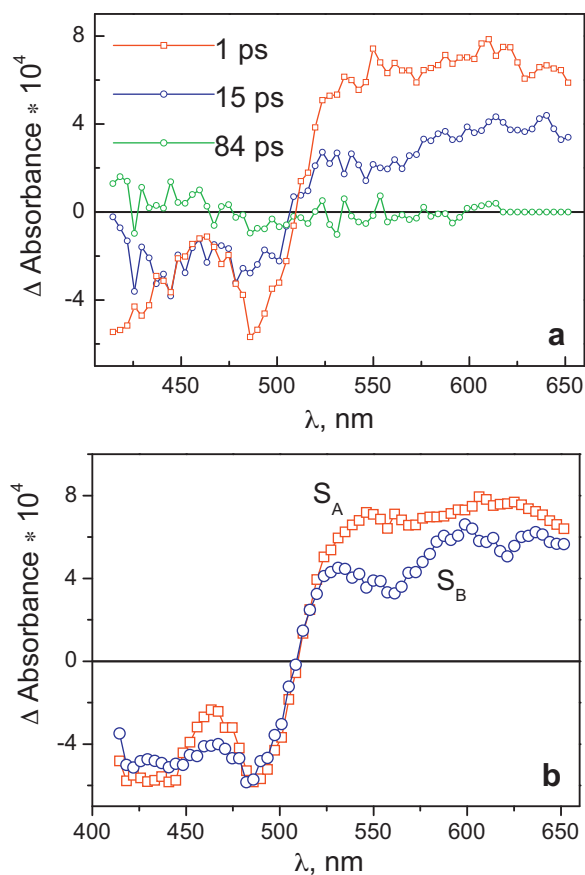$$S_B(\lambda) = A_2(\lambda)\frac{k_1 - k_2}{k_1} + A_3(\lambda)\frac{k_1 - k_3}{k_1} \tag{9}$$

$$S_C(\lambda) = A_3(\lambda)\frac{(k_1 - k_3)(k_2 - k_3)}{k_1 k_2} \tag{10}$$

In the case of the biexponential decay (6) the formulae for SADS corresponding to the sequential decay of the transient absorption $A \rightarrow B \rightarrow$ ground state are reduced to Eqs. (11) and (12).

$$S_A(\lambda) = A_1(\lambda) + A_2(\lambda) \tag{11}$$

$$S_B(\lambda) = A_2(\lambda)\frac{k_1 - k_2}{k_1} \tag{12}$$

Examples of the kinetic curves for the $IrCl_6^{2-}$ complex in methanol solutions are shown in Fig. 4 (dots). At all the wavelengths, the intermediate absorption completely disappeared in a time of ca. 70 ps. The initial parts of the kinetic curves (at time less than 0.8 ps, see the left-hand part of Fig. 4) are affected by the coherent artifact caused by the coherent interactions between pump and probe pulses [40]. The characteristic kinetic curves and chirp-corrected time-resolved spectra for the excitation of pure solvents are shown in Supplementary materials. The sets of the kinetic curves for $IrCl_6^{2-}$ in methanol and water were globally fitted using biexponential functions. To avoid the influence of the coherent artifact, the experimental points with the time delays from the laser pulse less than 0.8 ps were excluded from the fitting procedure. Therefore, in the case of UV excitation the existence of the coherent artifact imposes a limitation on the possibility to study the initial photophysical processes, which characteristic times are less than 1 ps. In the case of visible excitation of aqueous and alcohol solutions no coherent artifact was observed. When $IrCl_6^{2-}$ was excited in the visible region [26,27] biexponential or triexponential fittings

Fig. 5. ($\lambda_{pump} = 320$ nm) photolysis of $IrCl_6^{2-}$ (1.9×10^{-3} M) in methanol solution. (a)—intermediate absorption spectra at different times; (b)—species associated difference spectra (SADS) obtained from the biexponential global fit of kinetic curves (Fig. 4) and formulae (11) and (12).

Fig. 6. $IrCl_6^{2-}$ photolysis in aqueous (1 and 2) and methanol (3 and 4) solutions. Excitation at 320 nm for curves 1 and 3, 420 nm for curve 2, and 400 nm for curve 4. Curves 1–4 correspond to the SADS of the most stable intermediates. Curves 2 and 4 are matched to curve 1 at 610 nm. Data for the 400–420 nm excitation were taken from [26]. Possible transitions from the $1U_g{}'$ state are indicated.
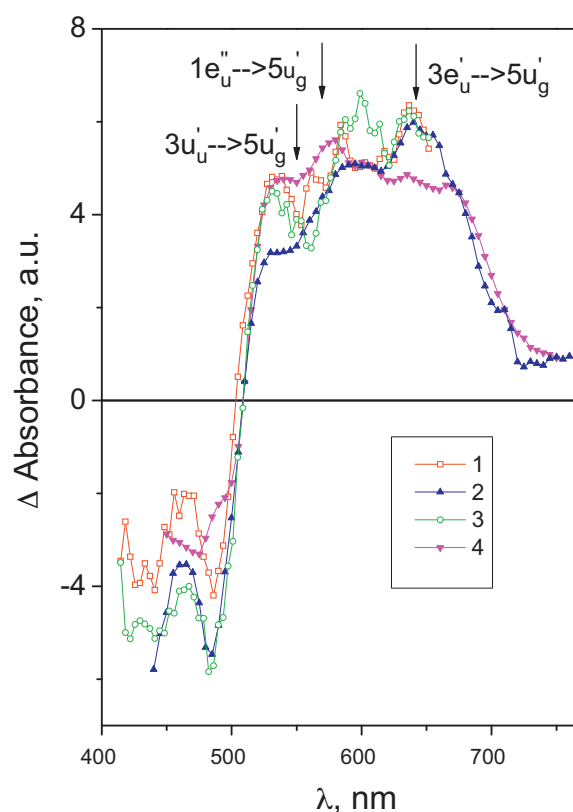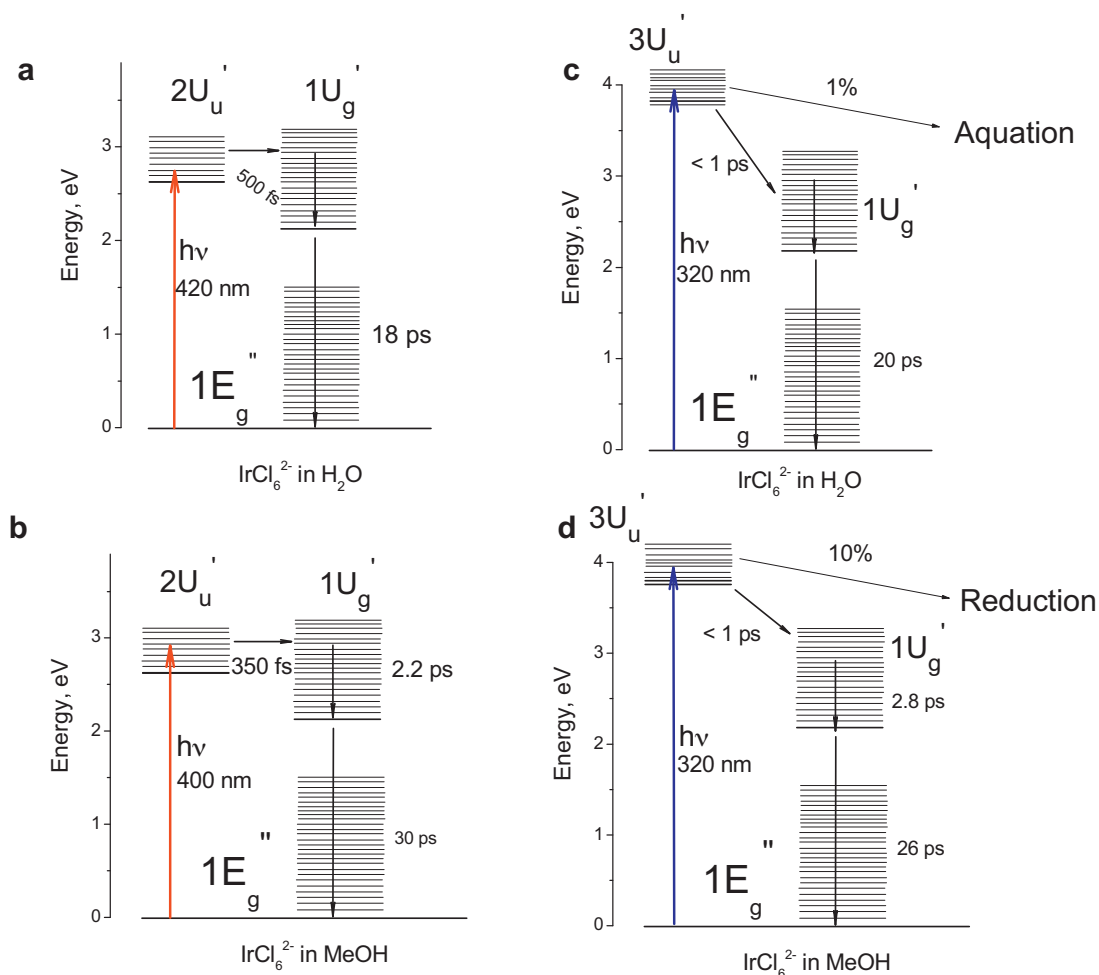
of the kinetic curves gave the opportunity to extract the lifetimes of the initial processes which were shorter than 1 ps (Table 2).

The best fits for methanol solutions of $IrCl_6^{2-}$ are presented in Fig. 4 as the solid curves. The longest characteristic time (Table 2) always lies in the region of 20–30 ps. In the case of $IrCl_6^{2-}$ excitation in methanol at 320 nm the first characteristic time (2.8 ps) could be extracted with confidence. The value of the first characteristic time in the case of aqueous solutions (0.6 ps) should be considered as a brief estimation because of very few points available to extract this time.

Fig. 5a demonstrates the differential intermediate absorption spectra for $IrCl_6^{2-}$ in methanol solution recorded at different time delays after the 320 nm excitation. Negative absorption at $\lambda < 510$ nm corresponds to the depletion of the ground state of the complex, and positive absorption at $\lambda > 510$ nm reflects the formation of the transient absorption.

The absorption spectrum at 84 ps (Fig. 5a) shows no evidence of the residual absorption caused by photoreduction of the initial complex. Because Ir(III) complexes have only weak d–d bands in the visible spectral region [41], one could expect the residual bleaching in the region of intense $IrCl_6^{2-}$ absorption (410–500 nm). The quantum yield of $IrCl_6^{2-}$ photoreduction in methanol at 308 nm excitation is 0.1 [37]. The maximal expected value of the bleaching, in conditions of the experiment described by Fig. 5a, is 5×10^{-5}. Such a low value of the differential absorption could not be extracted from the noisy experimental kinetic curves (Fig. 4).

The SADS corresponding to the consecutive short-living intermediates A and B are shown in Fig. 5b.

3.3. Comparison of $IrCl_6^{2-}$ excitation in the regions of visible LMCT bands and d–d bands

To compare transient absorption caused by $IrCl_6^{2-}$ excitation at the different spectral regions, the SADS corresponding to the final transient species are plotted in Fig. 6. For convenience, the amplitudes of the spectra obtained in different experiments are matched to the same scale. Curves 1–3 correspond to the species B formed in the two-stage process A → B→ ground state. In the case of $IrCl_6^{2-}$ photolysis in methanol at 400 nm the decay was found to be triexponential [27]. Correspondingly, curve 4 in Fig. 6 corresponds to the transient species C in the three-stage process A → B → C → ground state.

The similarity of curves 1–4 in Fig. 6 allows one to conclude that the final SADS in all the cases correspond to the same excited state. As it was proposed in [27], this state is the lowest electronic excited state of $IrCl_6^{2-}$, namely $1U_g{}'$, formed by the electronic configuration with a hole in $5u_g{}'$ orbital. According to [36], $1U_g{}'$ is a mixed metal-ligand state with ca. 50% of metal character lying ca. 5200 cm^{-1} higher than the ground state. In the framework of this interpretation the spectra 1–4 in Fig. 6 are caused by the transitions from the $1U_g{}'$ state. The wavelengths of the transitions corresponding to $3e_u{}' \rightarrow 5u_g{}'$, $1e_u{}'' \rightarrow 5u_g{}'$ and $3u_u{}' \rightarrow 5u_g{}'$ promotions (calculated using results of [35,36] and experimental spectrum in Figs. 1 and 2) are 641, 550 and 570 nm. The positions of these transitions are marked by arrows in Fig. 6. Therefore, the description of the observed final SADS of $IrCl_6^{2-}$ corresponding to 320 and 400 nm excitation is quantitative.

Now we can discuss the fastest processes followed by $IrCl_6^{2-}$ excitation. In the experiments performed with the visible LMCT

Fig. 7. Schematic representation of the processes followed by ultrafast excitation ((a)—420 nm, (b)—400 nm; (c) and (d)—320 nm) of $IrCl_6{}^{2-}$ in water ((a) and (c)) and methanol ((b) and (d)).

excitation (400–420 nm) the processes occurring in the first picosecond after the laser pulse were examined quantitatively [26,27]. Initially, vibrationally hot $(2U_u{}')^*$ excited state is formed. In alcohol solutions the $(2U_u{}')^*$ state transforms to the vibrationally hot lowest electronic excited state $(1U_g{}')^*$, which is followed by its vibrational cooling. The corresponding processes and characteristic lifetimes are shown in Fig. 7b and Table 2. The characteristic time of several hundreds of femtoseconds is typical for the electronic transitions in the metal complexes. The examples are presented in the reviews of Vlcek [42] and Forster [43] and references there.

In the case of aqueous solutions the characteristic lifetime of the $(1U_g{}')^*$ state vibrational cooling is less that in the case of alcohol solutions, therefore, electronic transition $(2U_u{}')^* \to (1U_g{}')^*$ and vibrational cooling of $(1U_g{}')^*$ appear as a single convoluted process (Fig. 7a). The situation when the different processes (e.g., intersystem crossing and vibrational relaxation) have similar characteristic times and manifest itself as a single, convoluted process often happens in photophysics of coordination compounds [42].

The tentative schemes of the processes occurring after the laser excitation are shown in Fig. 7. For simplification, only $2u_u{}' \to 2e_g{}''$ promotion (which plays the main role, as shown in Section 3.1) is marked for the 320 nm excitation. In the case of visible excitation 100% of the excited complex returned to the ground state. In the case of 320 nm excitation in aqueous solutions the quantum yield of the photochemical reaction is rather low (0.01, see Table 1). For methanol solutions the value of quantum yield is significantly higher (0.1, Table 1). In spite of that, the spectra and lifetimes of the

SADS corresponding to the last intermediate are similar (Fig. 6). This fact could be explained in two ways: (i) all the changes in the behavior of the excited complex caused by the differences in 400–420 and 320 nm excitation occur in the time interval of 1–3 ps; and/or (ii) the spectral signatures of the chemical processes do not fall to the probing range (400–650 nm) used in this work.

Unfortunately, in the case of 320 nm excitation the coherent artifact prevents the resolution of the spectra of the initially formed excited states. For the case of methanol solutions the first extracted characteristic lifetime (2.8 ps, Table 2 and Fig. 7d) corresponds to the vibrational cooling of the lowest $1U_g{}'$ excited state of the initial complex. The first argument in favor of this interpretation is the similarity of SADS corresponding to the discussed species A and B (Fig. 5b). Sharpening of the absorption bands for the species B is a feature of the vibrational relaxation, which could be accompanied by the solvent relaxation. Another argument in favor of the vibrational relaxation is the similarity of the corresponding lifetimes for the cases of visible and UV excitation.

When $IrCl_6{}^{2-}$ complex is excited at 320 nm in aqueous solutions, the formation time of vibrationally cooled $1U_g{}'$ state is less than 1 ps. The characteristic time extracted from the experimental data (0.6 ps, Table 2) should be considered as a brief estimation because there are too few experimental points for the determination of this time. As a matter of fact, vibrational relaxation of $IrCl_6{}^{2-}$ in aqueous solutions was not observed as a single, well-determined process both in the case of 420 and 320 nm excitation. The process of vibrational relaxation for aqueous solutions is

typically faster than for alcohol solutions [44,45]. In the case of the $IrCl_6^{2-}$ complex it manifests itself as a single process in alcohol but is convoluted with other processes in aqueous solutions. Therefore, the first characteristic time (estimated as 0.6 ps) includes the transition of the initially formed Franck-Condon state (hot $(3U_u')^*$ state for $2e_g'' \rightarrow 6u_g'$ promotion), its conversion to the hot lowest excited state $(1U_g')^*$, its vibrational cooling and solvent relaxation. The proposed pattern of the observed processes is shown in Fig. 7c.

4. Conclusions

In this paper, the primary photophysical processes for the excitation of the $IrCl_6^{2-}$ complex in the region of the visible LMCT bands (400–420 nm) and near UV band (320 nm), which is presumably LMCT with less than 20% addition of d–d transitions, were compared. Visible charge transfer bands of $IrCl_6^{2-}$ are not photoactive both in aqueous and alcohol solutions. Therefore, the experiments on femtosecond pump-probe spectroscopy with the visible excitation reflect the photophysical processes resulting in the recovery of the initial state. In the case of the UV (320 nm) excitation, $IrCl_6^{2-}$ is photoactive in aqueous and methanol solutions with the low quantum yields (0.01 and 0.1 correspondingly). The experiments have shown that the spectra of the most stable species occurring in all the studied systems are the same and correspond to the thermally relaxed lowest electronic excited state of $IrCl_6^{2-} - 1U_g'$. The thermally relaxed $1U_g'$ state is formed within 1–3 ps (depending on the solvent) after the laser pulse. After $1U_g'$ formation, its transition to the ground state is the only observed process. The chemical processes caused by the 320 nm excitation, namely photoaquation in water and photoreduction in alcohols (which are schematically shown in Fig. 7c and d) were not detected in the described experiments. This could be explained in two ways:

(a) All the processes determining the photochemical reactions occurred in the time interval of 1–3 ps, and they were not directly observed due to small quantum yields and coherent artifact formation;
(b) The spectral signatures of the chemical processes lie outside of the probing range (400–650 nm) used in this work, and in future the efforts to expand the probing range are necessary.

Acknowledgements

Appendix A. Supplementary data

Supplementary material related to this article can be found, in the online version, at http://dx.doi.org/10.1016/j.jphotochem.2014.07.011.

References

[1] J. Herschel, On the action of light in determining the precipitation of muriate of platinum by lime-water, Philos. Mag. 1 (1832) 58–60.
[2] V. Balzani, V. Carassiti, Photochemistry of Coordination Compounds, Acad. Press, New York, NY, 1970, pp. 307–312, 257–269.
[3] P.C. Ford, J.D. Peterson, R.E. Hintze, Photochemistry of hexacoordinate complexes of the heavier transition metals, Coord. Chem. Rev. 14 (1974) 67–105.
[4] A.W. Adamson, P.D. Fleischauer (Eds.), Concepts of Inorganic Photochemistry, Wiley, New York, NY (etc.), 1975.
[5] J. Sykora, J. Sima, Photochemistry of Coordination Compounds, Elsevier, Amsterdam, 1990.
[6] L. Zang, W. Macyk, C. Lange, W.F. Mayer, C. Antonius, D. Meissner, H. Kish, Visible-light detoxification and charge generation by transition metal chloride modified titania, Chem. Eur. J. 6 (2000) 379–384.
[7] W. Macyk, H. Kish, Photosensitization of crystalline and amorphous titanum dioxide by platinum(IV) chloride surface complexes, Chem. Eur. J. 7 (2001) 1862–1867.
[8] F.B. Li, X.Z. Li, The enhancement of photodegradation efficiency using Pt–TiO₂ catalyst, Chemosphere 48 (2002) 1103–1111.
[9] W. Macyk, G. Burgeth, H. Kish, Photoelectrochemical properties of platinum(IV) chloride surface modified TiO₂, Photochem. Photobiol. Sci. 2 (2003) 322–328.
[10] Q. Li, Zh. Chen, X. Zheng, Zh. Jin, Study of photoreduction of PtCl₆²⁻ on CdS, J. Phys. Chem. 96 (1992) 5959–5962.
[11] Zh. Jin, Zh. Chen, Q. Li, Ch. Xi, X. Zheng, On the conditions and mechanism of PtO₂ formation in the photoinduced conversion of H₂PtCl₆, J. Photochem. Photobiol. A: Chem. 81 (1994) 177–182.
[12] J. Pracharova, L. Zerzankova, J. Stepankova, O. Novakova, N.J. Farrer, P.J. Sadler, V. Brabec, J. Kasparkova, Interactions of DNA with a new platinum(IV) azide dipyridine complex activated by UVA and visible light: relationship to toxicity in tumor cells, Chem. Res. Toxicol. 25 (2012) 1099–1111.
[13] K.L. Swancutt, S.P. Mezyk, J.J. Kiddle, Free radical-induced redox chemistry of platinum-containing anti-cancer drugs, Radiat. Res. 168 (2007) 423–427.
[14] P.J. Bednarski, F.S. Mackay, P.J. Sadler, Photoactivable platinum complexes, Anti-Cancer Agents Med. Chem. 7 (2007) 75–93.
[15] G.R. Gale, E.M. Walker Jr., A.B. Smith, A.E. Stone, Antitumor and antimitogenic properties of the photochemical reaction product of ammonium hexchloroiridate(IV), Proc. Soc. Exp. Biol. Med. 136 (1971) 1197–1202.
[16] N. Cutillas, G.C. Yellol, C. de Haro, C. Vicente, V. Rodriguez, J. Ruiz, Anticancer cyclometallated complexes of platinum group metals and gold, Coord. Chem. Rev. 257 (2013) 2784–2797.
[17] Zh. Liu, P.J. Sadler, Organoiridium complexes: anticancer agents and catalysts, Acc. Chem. Res. 47 (2014) 1174–1185.
[18] Sh. Moromizato, Y. Hisamatsu, T. Suzuki, Y. Matsuo, R. Abe, S. Aoki, Design and synthesis of a luminescent cyclometalated iridium(III) complex having N,N-diethylamino group that stains acidic intracellular organelles and induces cell death by photoirradiation, Inorg. Chem. 51 (2012) 12697–12706.
[19] S.P.-Y. Li, T.-Sh. Ch, M.-W. Lau, Y.-W. Louie, S.H. Lam, K. Cheng, K.-W. Lo, Mitochondria-targeting cyclometallated Ir(III)-PEG complexes with tunable photodynamic activity, Biomaterials 34 (2013) 7519–7532.
[20] A.W. Adamson, A.H. Sporer, Photochemistry of complex ions. I. Some photochemical reactions of aqueous PtBr₆²⁻, Mo(CN)₈⁴⁻, and various Co(III) and Cr(III) complex ions, J. Am. Chem. Soc. 80 (1958) 3865–3870.
[21] I.P. Pozdnyakov, E.M. Glebov, V.F. Plyusnin, N.V. Tkachenko, H. Lemmetyinen, Primary processes in photophysics and photochemistry of PtBr₆²⁻ complex studied by femtosecond pump-probe spectroscopy, Chem. Phys. Lett. 442 (2007) 78–83.
[22] I.L. Zheldakov, M.N. Ryazantsev, A.N. Tarnovsky, Wavepacket motion via a conical intersection in the photochemistry of aqueous transition-metal dainios, J. Phys. Chem. Lett. 2 (2011) 1540–1544.
[23] I.L. Zheldakov, Ultrafast photophysics and photochemistry of hex coordinated bromides of Pt(IV), Os(IV), and Ir(IV) in the condensed phase studied by femtosecond pump-probe spectroscopy, in: Ph. D. Thesis, Bowling Green State University, Bowling Green, OH, USA, 2010.
[24] E.M. Glebov, A.V. Kolomeets, I.P. Pozdnyakov, V.F. Plyusnin, V.P. Grivin, N.V. Tkachenko, H. Lemmetyinen, Redox processes in photochemistry of Pt(IV) hexahaloid complexes, RSC Adv. 2 (2012) 5768–5778.
[25] E.M. Glebov, A.V. Kolomeets, I.P. Pozdnyakov, V.P. Grivin, V.F. Plyusnin, N.V. Tkachenko, H. Lemmetyinen, Chain processes in the photochemistry of Pt^IV halide complexes in aqueous solutions, Russ. Chem. Bull., Int. Edit. 62 (2013) 1540–1548.
[26] A.V. Litke, I.P. Pozdnyakov, E.M. Glebov, V.F. Plyusnin, N.V. Tkachenko, H. Lemmetyinen, Photophysics of IrCl₆²⁻ complex in aqueous solutions studied by femtosecond pump-probe spectroscopy, Chem. Phys. Lett. 477 (2009) 304–308.
[27] E.M. Glebov, A.V. Kolomeets, I.P. Pozdnyakov, V.F. Plyusnin, N.V. Tkachenko, H. Lemmetyinen, Ultrafast pump-probe spectroscopy of IrCl₆²⁻ complex in alcohol solutions, Photochem. Photobiol. Sci. 10 (2011) 1709–1714.
[28] C. Rensing, O.T. Ehrler, J.-P. Yang, A.-N. Unterreiner, M.M. Kappes, Photodissociation dynamics of IrBr₆²⁻ dianions by time-resolved photoelectron spectroscopy, J. Chem. Phys. 130 (234306) (2009) 1–8.
[29] V. Balzani, M.F. Manfrin, L. Moggi, Photochemistry of coordination compounds, XVI. Hexabromoplatinate(IV) and hexaiodoplatinate(IV) ions, Inorg. Chem. 6 (1967) 354–358.
[30] L. Moggi, G. Varani, M.F. Manfrin, V. Balzani, Photochemical reactions of hexachloroiridate(IV) ion, Inorg. Chim. Acta 4 (1970) 335–341.
[31] E.M. Glebov, V.F. Plyusnin, N.V. Tkachenko, H. Lemmetyinen, Laser flash photolysis of IrCl₆²⁻ in aqueous solutions, Chem. Phys. 257 (2000) 79–89.
[32] S.V. Chekalin, The unique femtosecond spectroscopic complex as an instrument for ultrafast spectroscopy, femtochemistry and nanooptics, Phys. Usp. 49 (2006) 634–641.
[33] E.N. Sloth, C.S. Garner, Exchange of radioiridium between hexachloroiridate(III) and hexachloroiridate(IV) ions, J. Am. Chem. Soc. 77 (1955) 1440–1444.
[34] C.K. Jørgensen, Electron transfer spectra of hexahalide complexes, Mol. Phys. 2 (1959) 309–332.
[35] A. Goursot, H. Chermette, C. Daul, Relativistic calculation of the electronic structure and related properties of IrCl₆²⁻, Inorg. Chem. 23 (1984) 305–314.
[36] J.P. Lopez, D.A. Case, Relativistic scattered wave calculations of hexachloro- and hexabromoiridate(IV), J. Chem. Phys. 81 (1984) 4554–4563.
[37] E.M. Glebov, V.F. Plyusnin, N.I. Sorokin, V.P. Grivin, A.B. Venediktov, H. Lemmetyinen, Photochemistry of IrCl₆²⁻ complex in alcohols, J. Photochem. Photobiol. A: Chem. 90 (1995) 31–37.

[38] E.M. Glebov, V.F. Plyusnin, V.P. Grivin, Yu.V. Ivanov, N.V. Tkachenko, H. Lemmetyinen, Photoreduction of $IrCl_6^{2-}$ complex in alcohol solutions and its reaction with hydroxyalkyl radicals, Int. J. Chem. Kinet. 30 (1998) 711–720.

[39] A.S. Rury, R.J. Sension, Broadband ultrafast transient absorption of iron(III) tetraphenylporphyrine chloride in the condensed phase, Chem. Phys. 422 (2013) 220–228.

[40] L. Palfrey, T.F. Heinz, Coherent interactions in pump–probe absorption measurements: the effect of phase gratings, J. Opt. Soc. Am. B: Opt. Phys. 2 (1985) 674–679.

[41] I.A. Poulsen, C.S. Garner, A. Thermodynamic, Kinetic study of hexachloro and aquapentachloro complexes of iridium(III) in aqueous solutions, J. Am. Chem. Soc. 84 (1962) 2032–2037.

[42] A. Vlcek Jr., The life and times of excited states of organometallic and coordination compounds, Coord. Chem. Rev. 200–202 (2000) 933–978.

[43] L.S. Forster, Intersystem crossing in transition metal complexes, Coord. Chem. Rev. 250 (2006) 2023–2033.

[44] J.L. Perez Lustres, S.A. Kovalenko, M. Mosquera, T. Senyushkina, W. Flasche, N.P. Ernsting, Ultrafast solvation of *N*-methyl-6-quinone probes local IR spectrum, Angew. Chem. Int. Ed. 44 (2005) 5635–5639.

[45] K. Dahl, G.M. Sando, D.M. Fox, T.E. Sutto, J.C. Owrutsky, Vibrational spectroscopy and dynamics of small anions in ionic liquid solutions, J. Chem. Phys. 123 (084504) (2005) 1–11.